SCIENTIFIC REPORTS

OPEN

The high efficient catalytic properties for thermal decomposition of ammonium perchlorate using mesoporous ZnCo$_2$O$_4$ rods synthesized by oxalate co-precipitation method

Xuechun Xiao[1,2], Bingguo Peng[1], Linfeng Cai[1], Xuanming Zhang[1], Sirui Liu[1] & Yude Wang[1,2]

Mesoporous ZnCo$_2$O$_4$ rods have been successfully prepared via oxalate co-precipitation method without any template. The nano-sized spinel crystallites connected together to form mesoporous structure by annealing homogeneous complex oxalates precursor at a low rate of heating. It is found that the low anneal rate plays an important role for the formation of mesoporous ZnCo$_2$O$_4$ rods. The effects of the heat temperature on the phase, morphology and catalytic properties of the products were studied. The XRD, SEM TEM, and N$_2$ absorption/desorption have been done to obtain compositional and morphological information as well as BET surface area of the as-prepared sample. Catalytic activities of mesoporous ZnCo$_2$O$_4$ rods toward the thermal decomposition of ammonium perchlorate (AP) were investigated with differential scanning calorimetry (DSC) and thermogravimetry (TG) techniques. The results show that the addition of ZnCo$_2$O$_4$ rods to AP dramatically reduces the decomposition temperature. The ZnCo$_2$O$_4$ rods annealed at 250 °C possesses much larger specific area and exhibits excellent catalytic activity (decrease the high decomposition temperature of AP by 162.2 °C). The obtained mesoporous ZnCo$_2$O$_4$ rods are promising as excellent catalyst for the thermal decomposition of AP.

Due to their various applications including propulsion for large space vehicles and tactical missiles, gas generators for airbags, composite solid propellants are being intensively pursued[1–3]. Ammonium perchlorate (AP), as the main high energy constituent of solid propellants in the national defense field, accounts for 60–90% of the total weight of composite propellants[4]. Hence, the burning velocity and energy features of the propellants are significantly affected by the decomposition of AP. A comprehensive research about the thermal decomposition of AP was carried out by researchers[5]. Results indicate that a small quantity of catalysts can reduce the thermal decomposition temperature of AP, especially that corresponding to the high temperature decomposition (HTD), boosting up the apparent decomposition heat of AP, and increasing the burning velocity and efficiency of propellant accordingly. Recently, various kinds of transition metal oxides have been explored as catalyst for use in the thermal decomposition of AP, primarily including Fe$_2$O$_3$, CuO, Co$_3$O$_4$, NiO, ZnO and other metal oxide powders[6–9]. Compared to the single metal oxide, the complex oxides (containing two or more types of cations) with spinel structure have allured a lot of attention in material research because that the stabilization of active phases and synergistic interactions between two different oxides may improve its catalytic performance[10–12]. The presence of a partially filled-3d orbital in CuCo$_2$O$_4$ structure, so easy to accept electrons and improve the transferring electrons from perchlorate ions to the ammonium ions, which exhibits its stronger catalytic activity than probably

[1]School of Materials Science and Engineering, Yunnan University, 650091, Kunming, People's Republic of China. [2]Department of Physics, Yunnan University, 650091, Kunming, People's Republic of China. Correspondence and requests for materials should be addressed to Y.W. (email: ydwang@ynu.edu.cn)

CuO and Co_3O_4 as reported by Gheshlaghi *et al*.[13]. On account of the synergistic effect between Cu^{2+} and Cr^{3+} in the $CuCr_2O_4$ nanoparticles, the $CuCr_2O_4$ exhibits better catalytic effect than CuO[14,15].

As a binary oxide, $ZnCo_2O_4$ is an attractive material with the bivalent Zn-ions occupying the tetrahedral sites in the cubic spinel structure and the trivalent Co-ions occupying the octahedral sites. $ZnCo_2O_4$ has recently attracted more and more attention for applying in catalyst in thermal decomposition of AP, owing to its excellent physicochemical performance and its abundant resources, low cost and environmental friendliness[16,17]. Porous structured materials have gained great attention for their superior physicochemical characters, including large specific area, high porosity, low density, high permeability and high adsorption performance. Hence, reports are available on the application of this type of materials in catalyst, for the fact that it favors the exposure of active sites and offer rapid mass transfer processes[18,19]. So it is an important part of this article to make further improvement on the catalytic activities of AP by introducing porous structure into spinel $ZnCo_2O_4$. Up to now, most approaches towards porous materials focus on template-assisted processes, including hard templates (porous silicon and polystyrene sphere) and soft templates (surfactants and block copolymers). Tomboc *et al*. synthesized hierarchical mesoporous $ZnCo_2O_4$ via using PVP as the soft template[20]. Highly ordered mesoporous spinel $ZnCo_2O_4$ with high surface area and narrow pore size was synthesized by using SBA-15 as the hard templates[21]. However, this synthetic route involves multi-step process, which is time-consuming and relatively complicated. So, it is very necessary to look for a simple and effective method to synthesize porous structure $ZnCo_2O_4$. A facial oxalate co-precipitation method to fabricate mesoporous spinel Co_3O_4 and $MCo_2O_{4(4.5)}$ (M = Mn, Ni, Fe, Cu) with high surface areas by a controlled pyrolytic of metal oxalate precursor as reported in[19,22]. This strategy is simpler and more efficient compared with other porous-casting method.

In this paper, the mesoporous $ZnCo_2O_4$ rod has been successfully synthesized via oxalate co-precipitation method without any template. The nano-sized spinel crystallites connected together to form mesoporous structure by annealing homogeneous complex oxalates precursor at a low rate of heating. The effects of the heat temperature on the phase, morphology and catalytic properties of the products were studied. The composition, morphology, porous structure, surface area and the catalytic activities to AP's thermal decomposition of as-prepared mesoporous $ZnCo_2O_4$ rod are investigated in detail. The preliminary analysis of catalytic mechanism is discussed.

Experimental

All the reagents used in the experiments were purchased from commercial sources of analytical grade and used without further purification.

Preparation of mesoporous $ZnCo_2O_4$ rod. The typical procedure adopted for the preparation of mesoporous $ZnCo_2O_4$ rod is as follows: 16 mM $Co(NO_3)_2 \cdot 6H_2O$ and 8 mM $Zn(NO_3)_2 \cdot 6H_2O$ were successively dissolved in 80 mL deionized water followed by magnetic stirring for 30 min to obtain a homogeneous solution. Subsequently, the 24 mL saturated sodium oxalate solutions was added slowly. After continuous stirring for 2 h, the precipitate was collected by centrifugation and washed with deionized water and absolute ethanol several times and dried in air at 60 °C overnight.

Afterward, the pink precursor was annealed at various temperature (250 °C, 300 °C, 350 °C and 400 °C) for 2 h at a lower heating rate (1 °C/min) in temperature programming furnace. After that, the product was cooled inside the furnace to room temperature. The resultant black powder was collected and directly subjected to the various characterizations.

Characterization of mesoporous $ZnMCo_2O_4$ rod. X-ray powder diffraction (XRD) patterns of the product was carried out on a Rigaku D/max-3B diffractometer with an incident X-ray wavelength of 1.540 Å (Cu Kα line), operated at 40 kV, 100 mA. The morphology was observed using field emission scanning electron microscopy (FESEM) taken on FEI nova nanosem 450 with microscope operating at 30 kV. Detailed studies of the microstructure were also carried out by transmission electron microscopy (TEM) (JEOL JEM-2100) at an acceleration voltage of 200 kV. XPS was carried out at room temperature in a PHI 5500 spectrometer with polychromatic Al/Mg-Kα X-ray source. During XPS analysis, Al Kα X-ray beam was adopted as the excitation source and power was set to 250 W. Vacuum pressure of the instrument chamber was 1×10^{-7} Pa as read on the panel. Measured spectra were decomposed into Gaussian components by a least-square fitting method. Bonding energy was calibrated with reference to C1s peak (285.0 eV). The pore size distributions and the BET surface areas were measured by nitrogen adsorption/desorption using a NOVA2200e gas sorption analyzer (Quantachrome Corp.). Prior to the measurements, the sample was degassed at 300 °C in vacuum for 3 h. The functional groups and coordination of the samples were studied via the FT-IR analysis performed on the Nicolet iS 10 (Semerel technology Corp.), the frequency is range from 4000 to 400 cm^{-1}. Thermogravimetric and differential thermal analysis (TG-DTA) were performed on a HCT-3 thermal analyzer (Bei-jing) at a heating rate of 10 °C/min from 25 °C to 400 °C.

Catalytic performance to thermal decomposition of AP. The as-prepared sample was mixed with AP to reach certain mass ratios of 2%, 5%, 7% and 10%, respectively. The mixture was fully grinded in the presence of a certain amount of anhydrous ethanol until the ethanol volatilize. Afterwards, the catalytic activities of mesoporous $ZnCo_2O_4$ rod in the thermal decomposition of AP were performed using a HCT-3 thermal analyzer (Bei-jing) at a heating rate of 20 °C/min in nitrogen atmosphere over the range of 25–500 °C.

Results and Discussion

Researches show that the pyrolytic process of precipitated precursors has a strong effect on the crystallite phase and the morphology features (crystallite size, surface area, etc.) of the product[23]. Therefore, the pyrolytic behavior of homogeneous complex oxalates precursor was first explored by TG-DTA analysis in air atmosphere, the results
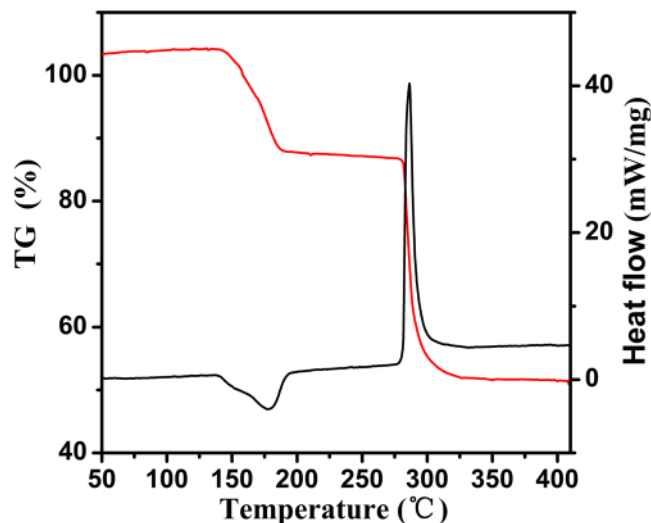
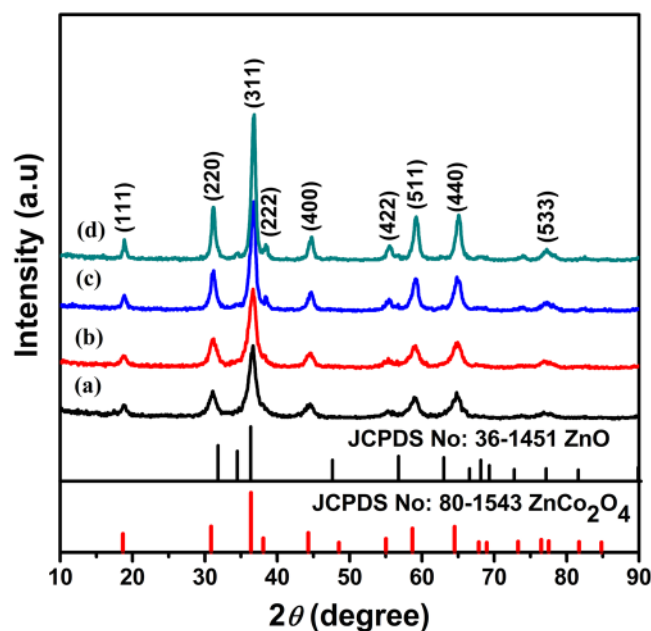**Figure 1.** The TG and DTA curves for as-prepared precursor.

Figure 2. The XRD pattern of the $ZnCo_2O_4$ at different calcined temperature: (**a**) 250 °C, (**b**) 300 °C, (**c**) 350 °C and (**d**) 400 °C, respectively.

of which is showed in Fig. 1. From the DTA curve, it can be seen that the endothermic process (the coordinated water elimination) happens at about 177 °C, and the precipitated precursor lost 12% of its original weight in the endothermic step as revealed by the TG curve. With increasing temperature, there is a rapid decline in mass (approximately 48% of its original) shown in the TG curve, which indicates the decomposition of oxalic groups and oxidation of the precursor into crystalline $ZnCo_2O_4$. This transitional process is accompanied by a strong exothermic peak at approximately 285 °C in the DTA curve. The single-phase feature of cobalt-zinc complex oxalate is further confirmed by the phenomenon that only one dehydration and one decomposition stage can be observed, as the endothermic and exothermic peaks of zinc oxalate do not accord with those of cobalt. Thus, it can be concluded that the zinc and cobalt atoms distribute on a molecular level in the resulting oxide lattice[19]. The decomposition temperature has huge effect on the crystalline size and the surface area of the resulting sample, and the anneal temperature can be reduced finely with the heating rate decreasing[22,23]. Hence, in this paper, in order to unveil the effects of the heat temperature on the phase, morphology and catalytic properties of the products, the pyrolysis temperature was set at various values from 250 °C to 400 °C on the basis of the above TG-DTA analysis.

XRD patterns of final products obtained by sintering the precursor at 250 °C, 300 °C, 350 °C and 400 °C are shown in Fig. 2(a–d) correspondingly. All the diffraction peaks of the samples are in good consistency with the
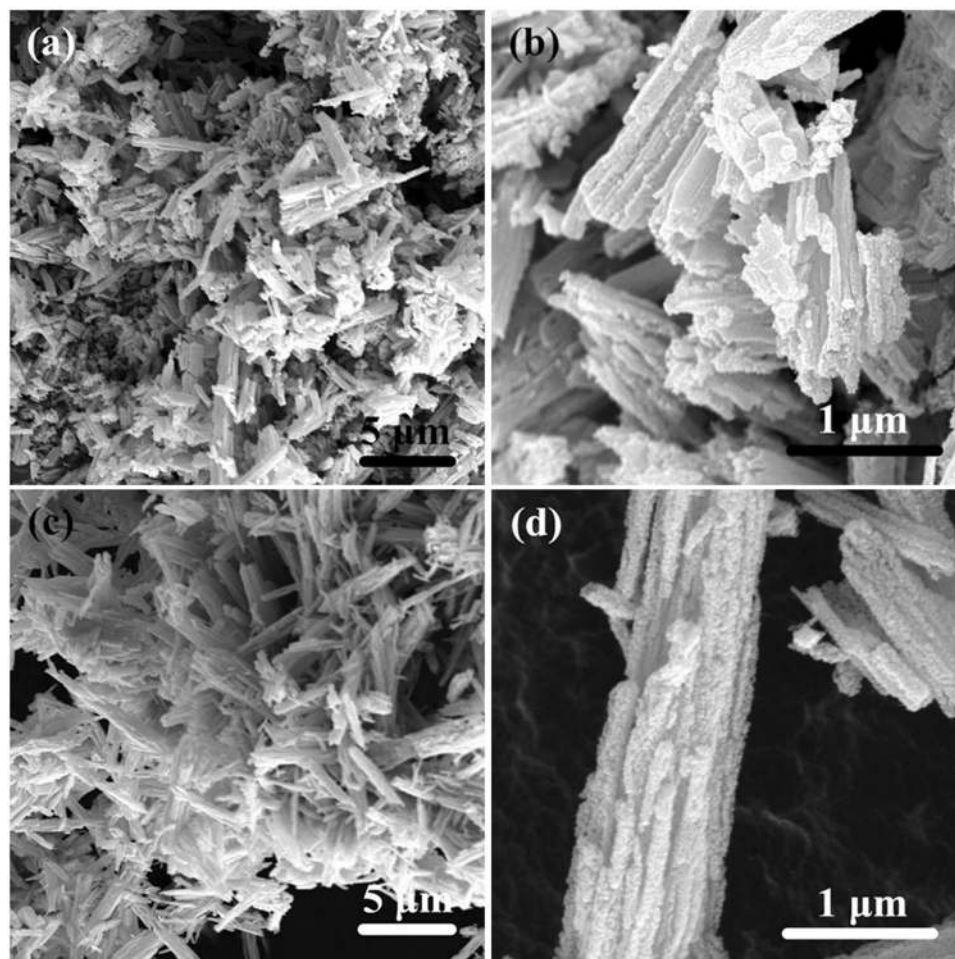
Figure 3. FESEM images of the ZnCo₂O₄ at different calcined temperature: (**a**) and (**b**) 250 ℃, (**c**) and (**b**) 400 ℃, respectively

that of spinel $ZnCo_2O_4$ (JCPDS card no. 80-1543). It also can be seen that the diffraction peaks become increasingly sharp as the calcination temperature elevating, which confirms better crystallization and bigger grain size of the decomposed products with the temperature elevating. But there are diffraction peaks originating from the other phases besides the pure $ZnCo_2O_4$ phase (curve (c,d) in Fig. 2) in the XRD spectrum when the heat temperature increases. The peak positions of the additional phases agree with the standard values of the wurtzite ZnO (JCPDS No. 36-1451).

Surface morphologies of the as-synthesized $ZnCo_2O_4$ calcined at 250 °C and 400 °C are studied with FESEM, and the obtained results are shown in Fig. 3. Figure 3(a,b) reveals the LRSEM and HRSEM images of the product calcined at 250 °C, and Fig. 3(c,d) corresponds to 400 °C. From the Fig. 3, it can be seen that the morphology of the pyrolysis products are nano-sized crystallites connected together to form mesoporous rod structure, and no obvious changes of the integral structure are observed as the heating temperature increases.

The more information about the shape and crystallite size of the calcined products were further analysed by TEM (Fig. 4). Figure 4(a,b) display the TEM images of the sample calcined at 250 °C with low and high magnification, respectively. From these images it can be seen that the as-synthesized $ZnCo_2O_4$ nano-crystals interconnected together to form porous structure. The low and high magnification TEM images of the $ZnCo_2O_4$ annealed at 400 °C are exhibited in Fig. 4(c,d). These images demonstrate that the overall porous structure did not change at all, while enlargement of the crystalline size can be observed. In addition, lattice spacing between adjacent planes measured in the high-resolution TEM images (Fig. 4(b,d)) is 0.470 nm, and 0.462 nm, showing agreements with the distance between (111) crystal planes of cubic spinel $ZnCo_2O_4$. The porous structure might be formed by large amounts of gases slowly released from the micrometer sized oxalate particles leaving over plenty of space during the pyrolysis process[19].

The pore size distribution and surface area of the as-synthesized $ZnCo_2O_4$ obtained at different calcination temperature were measured by nitrogen adsorption/desorption method at 77 K. Figure 5 are N_2 adsorption-desorption isotherms and corresponding pore size distribution plots (plotted by using the BJH calculation model) of the as-synthesized $ZnCo_2O_4$. As can be seen in Fig. 5, all of the porous $ZnCo_2O_4$ calcined at different temperatures exhibit a type IV isotherms and H3 hysteresis loop according to the IUPAC classification, which suggest that the mesoporous structure is formed by slit-like mesopore. Those pores were produced form
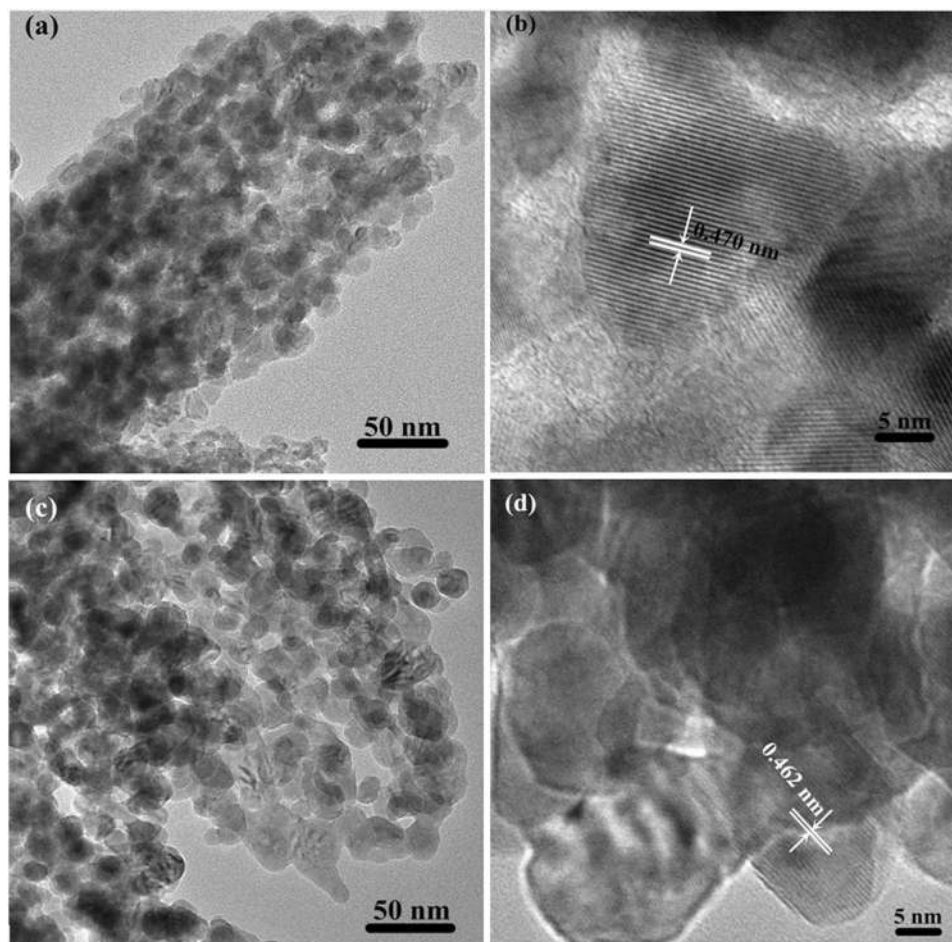
Figure 4. TEM and HRTEM images of the $ZnCo_2O_4$ at different calcined temperature: (**a**) and (**b**) 250 °C, (**c**) and (**b**) 400 °C, respectively.

the decomposition of cobalt - zinc oxalate hydrate crystallization during the pyrolysis process. The structural parameters and BET specific surface areas of the as-prepared $ZnCo_2O_4$ are derived from the isotherms and tabulated in Table 1. The BET surface areas of $ZnCo_2O_4$ calcined at 250 °C, 300 °C, 350 °C, 400 °C are determined to be 102.34, 101.36, 68.02 and 43.25 $m^2 \cdot g^{-1}$, respectively. The above data show that the calcination temperature has a significant impact on the specific surface areas of the products, i.e., the high calcination temperature will induce extensive growth of the spinel $ZnCo_2O_4$ and the collapse of the pore network. Thus, the specific surface area of $ZnCo_2O_4$ calcined at 400 °C dropped to 43.25 $m^2 \cdot g^{-1}$. From the pore size distribution curve (embedding figure in Fig. 5), it can be seen the size of pores exhibits a strong peak between 2.0 nm to 50 nm for the $ZnCo_2O_4$ calcined at different temperature, further verifying the presence of the mesoporous structure in the as-synthesized $ZnCo_2O_4$. The BJH pore volume of $ZnCo_2O_4$ calcined at 250 °C, 300 °C, 350 °C, 400 °C is 0.256, 0.294, 0.275 and 0.261 $cm^3 \cdot g^{-1}$ based on the calculation, respectively.

The chemical states and surface properties of as-synthesized $ZnCo_2O_4$ calcined at 250 °C were analyzed via X-ray photoelectron spectroscopy (XPS), as shown in Fig. 6. Figure 6(a) shows a full survey spectrum of the $ZnCo_2O_4$ rod. Characteristic peaks for Zn, Co, O and C elements can be observed in the obtained curve. The binding energy values of the major peaks are 780.5 and 795.5 eV in the Co 2p spectrum (Fig. 6(b)), corresponding to Co 2p3/2 and Co 2p1/2, respectively. Additionally, the spine-orbit splitting of the mentioned two peaks is 15.0 eV, in accordance with data reported in the literatures[24,25]. Two accompanied weak satellite peaks located at 790.1 and 805.4 eV can also be observed, and the energy gap between the main peak and the satellite peaks is around 9.6 eV. This suggests that Co cation should be trivalent[26]. The strong resolution Zn 2p spectrum is presented in (Fig. 6(c)), in which two strong peaks at 1021.50 and 1044.50 eV can be clearly seen, corresponding to the binding energy of Zn $2p_{3/2}$ and Zn $2p_{1/2}$, respectively, indicating the presence of Zn^{2+} in the $ZnCo_2O_4$ structure. It is observed that there is an energy separation of 23 eV between the Zn $2p_{3/2}$ and Zn $2p_{1/2}$ peaks, which is in agreement with an earlier report on $ZnCo_2O_4$[27]. From the O1s spectrum (Fig. 6(d)), it can be seen that the spectrum can be fitted to two gauss peaks at 529.8 eV and 531.7 eV are attributed to the lattice oxygen from the $ZnCo_2O_4$ rod and the oxygen from hydroxide ions[28].

The FT-IR spectrum of the as-synthesized $ZnCo_2O_4$ rod calcined at 250 °C was displayed in the Fig. 7. The characteristic band around 3442 cm^{-1} is assigned to the stretching vibration mode of H-O-H group, indicating the presence of chemisorbed water molecules. The prominent band of CO_3^{2-} ions at 1634 cm^{-1} and the
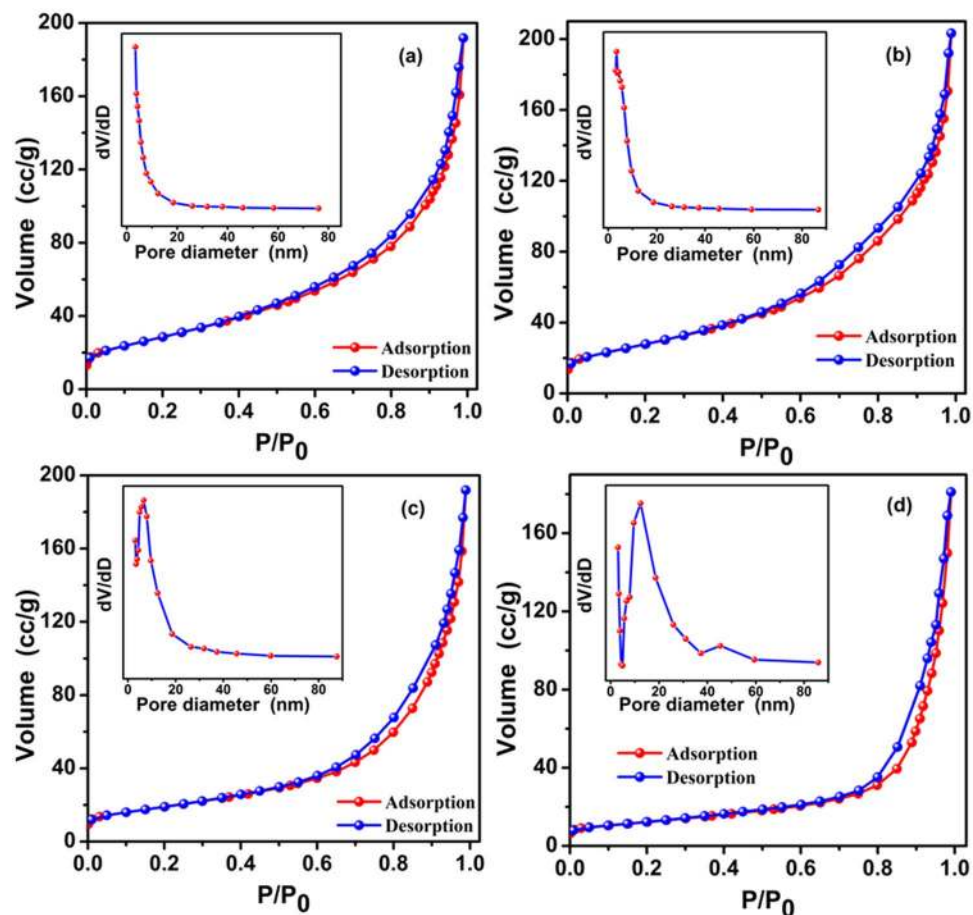
Figure 5. Nitrogen adsorption-desorption isotherm of $ZnCo_2O_4$ at different calcined temperature: (**a**) 250 °C, (**b**) 300 °C, (**c**) 350 °C and (**d**) 400 °C, respectively. Insert is the pore-size distribution calculated by the BJH method from the desorption branch of the $ZnCo_2O_4$.

Samples	BJH pore size (nm)	BJH pore volume (cm³/g)	BET specific surface area (m²/g)
$ZnCo_2O_4$ (250 °C)	3.410	0.256	102.335
$ZnCo_2O_4$ (300 °C)	5.618	0.294	101.358
$ZnCo_2O_4$ (350 °C)	7.829	0.275	68.021
$ZnCo_2O_4$ (400 °C)	12.379	0.261	43.247

Table 1. The structural parameters and BET specific surface area of $ZnCo_2O_4$ at different calcined temperature.

symmetric vibration ν_{sym} (COO⁻) at 1390 cm⁻¹ were observed[29]. The bands at 666 and 566 cm⁻¹ can be assigned to the metal-oxygen vibration frequency of the metal at tetrahedral clearance (Zn-O) and octahedral clearance (Co-O), indicating the formation of $ZnCo_2O_4$ spinel structure[30].

The propellant's burning rate is affected by the AP particle size[31,32], the particle size of AP is studied through SEM before the thermal decomposition analysis. From the SEM images of pure AP (Fig. S1.), the AP was inhomogeneous bulk structure, and its size was micron level, from tens of micron to few hundreds micron.

The catalytic performance of as-prepared $ZnCo_2O_4$ in the thermal decomposition of AP is demonstrated by the DSC analysis. The curves of AP decomposition in the absence and presence of $ZnCo_2O_4$ rod calcined at different temperature at a 2% mass basis are shown in Fig. 8. For pure AP (Fig. 8(a)), the curve indicates that the decomposition process of AP consists of three stages. In first stage, the endothermic peak demonstrates that AP undergoes a crystallographic transition from orthorhombic to cubic phase at 243.47 °C[33], In the subsequent two stages, the following partial decomposition of AP at 336.76 °C is revealed by the low temperature decomposition (LTD) peak. After that, complete decomposition at 471.15 °C is revealed by the high temperature decomposition (HTD) peak[13]. Compared with the pure AP, an obvious difference for AP decomposition in the presence of mesoporous $ZnCo_2O_4$ rod with a mass ratio of 2% can be seen in Fig. 8. All of curves show endothermic peak at the almost same temperature, which indicates that the crystallographic phase transition hasn't been affected by the addition of the mesoporous $ZnCo_2O_4$ rod, while significant declines in the value of temperature can be
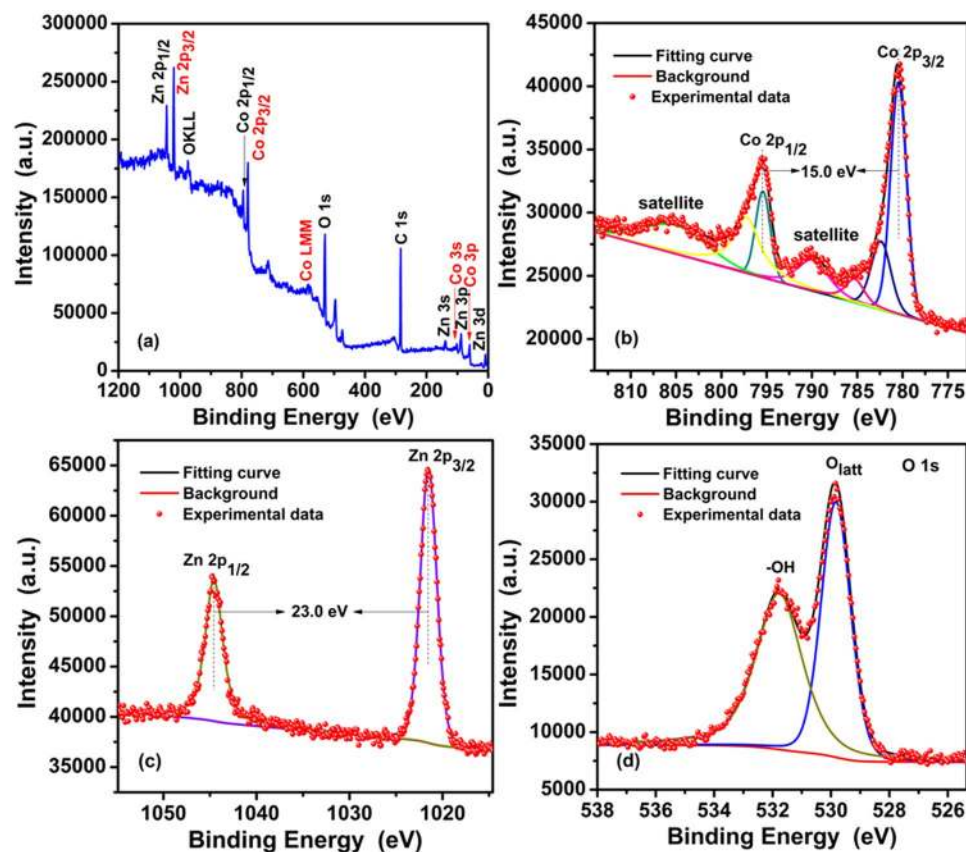
Figure 6. XPS spectra: (**a**) survey spectrum, (**b**) Co 2p, (**c**) Zn 2p, and (**d**) O 1s for the as-synthesized $ZnCo_2O_4$ calcined at 250 ℃.
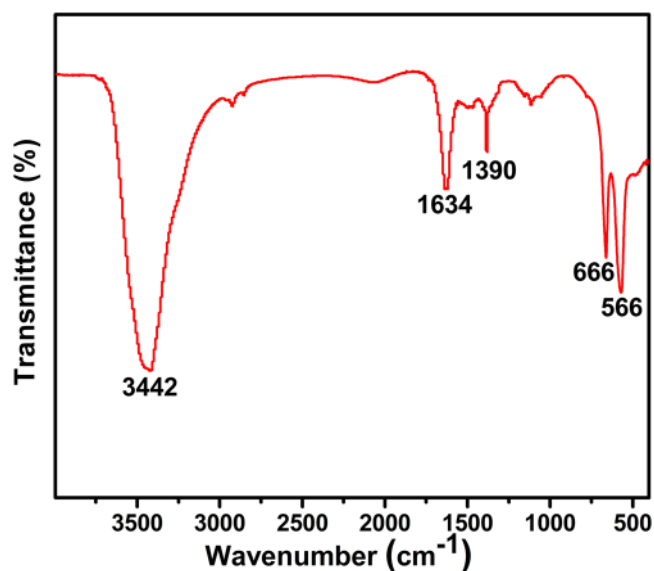

Figure 7. Typical FT-IR spectrum of the as-synthesized $ZnCo_2O_4$ calcined at 250 ℃.

seen from LTD and HTD peaks (Fig. 8(b–e)). All of the HTD peaks of AP in the presence of the mesoporous $ZnCo_2O_4$ rod shifted even to the front of the LTD peaks of pure AP, indicating that the mesoporous $ZnCo_2O_4$ rod can immensely promote the thermal decomposition of AP. The specific thermal decomposition temperature data are summarized in Table 2. The HTD peaks of AP containing the 2% mesoporous $ZnCo_2O_4$ rod calcined at 250, 300, 350, and 400 ℃ as catalyst are 308.93, 310.61, 314.26 and 315.73 ℃, respectively. These data show a decrease of 162.22, 160.54, 156.89 and 155.42 ℃ with respect to the pure AP. The results endorse the best
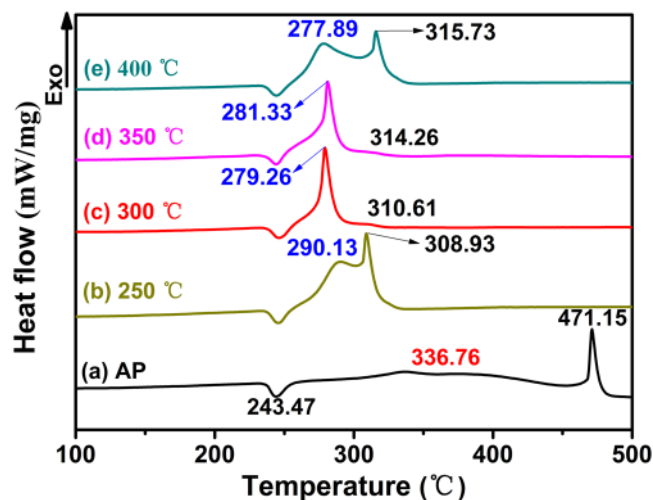
Figure 8. DSC curves of the AP decomposition in the absence and presence of $ZnCo_2O_4$ rod at different calcined temperature at a 2% mass basis: (**a**) pure AP, (**b**) 250 ℃, (**c**) 300 ℃, (**d**) 350 ℃ and (**e**) 400 ℃, respectively.

Samples	PT Peak (°C)	LTD Peak (°C)	HTD Peak (°C)
Pure AP	243.47	336.68	471.15
$ZnCo_2O_4$ (250 °C)	244.98	290.13	308.93
$ZnCo_2O_4$ (300 °C)	244.98	279.26	310.61
$ZnCo_2O_4$ (350 °C)	244.77	281.33	314.26
$ZnCo_2O_4$ (400 °C)	244.34	277.89	315.73

Table 2. Data of the AP decomposition in the absence and presence of $ZnCo_2O_4$ (2%) at different calcined temperature. Notes: In this table, PT, LTD and HTD represent crystallographic transition endothermic peak temperature, low-temperature decomposition and high-temperature decomposition respectively.

catalytic performance of mesoporous $ZnCo_2O_4$ rod calcined at 250 °C. It is reasonable to propose that the relatively highest specific surface area and the lowest pore size of $ZnCo_2O_4$ rod calcined at 250 °C might be the origin of its extraordinary performance, as those paramaters are all crucial factors affecting of catalytic efficiency. From the TG curves (Fig. 9), it can be seen that within the scope of 100 °C to 500 °C, two weight loss steps are clearly observed for pure AP. The first weight loss can be attributed to the partial decomposition of AP and formation of some intermediates by dissociation and sublimation. The second weight loss is caused by the complete decomposition of the intermediate to volatile products[34]. Whereas only one weight loss presents in the decomposition of AP with 2% mesoporous $ZnCo_2O_4$ rod (w/w), indicating that the final decomposition temperature of AP had been significantly decreased by the additive mesoporous $ZnCo_2O_4$ rod calcined at different temperature (pure AP: 474.41 °C, AP + 2%$ZnCo_2O_4$ (400 °C): 329.62 °C, AP + 2%$ZnCo_2O_4$ (350 °C): 328.89 °C, AP + 2%$ZnCo_2O_4$ (300 °C): 296.71 °C, AP + 2%$ZnCo_2O_4$ (250 °C): 292.71 °C). This phenomenon considerably concurs with the exothermic peaks of the DSC curves. It can be seen that the mesoporous $ZnCo_2O_4$ rod calcined at 250 °C manifests highest catalytic activity. In addition, the catalytic activity of the mesoporous $ZnCo_2O_4$ rod are the highest than those reported in literatures[5,13,17,35–39], as shown in Table 3.

The thermal decomposition of AP is also influenced by the blend ratio of mesoporous $ZnCo_2O_4$ rod. DSC curves of AP with a different mass ratio of mesoporous $ZnCo_2O_4$ rod calcined at 250 °C and pure AP are shown in Fig. 10. From Fig. 10, obvious changes can be observed in AP with the addition of mesoporous $ZnCo_2O_4$ rod (calcined at 250 °C) of different weight ratios. The HTD peaks of AP are lowered with the increasing mass ratio of the mesoporous $ZnCo_2O_4$ rod additive (from 308.93 °C at 2% mass ratio to 295.98 °C at 10% mass ratio). The results reveal that better catalytic performance is achieved with mesoporous $ZnCo_2O_4$ within the mixture. TG curves of pure AP and mixtures of $ZnCo_2O_4$ and AP with different mass ratios are given in Fig. 11. Two weight loss steps are present during the decomposition of AP, whereas only one step can be observed for mixtures according to the TG curves. Moreover, the temperature corresponding to the start of significant weight loss for mixtures decreases with increased the mass ratios. This finding considerably agrees with that derived from Fig. 10.

Up to now, the thermal decomposition mechanism of AP is not yet fully understood because the decomposition process of AP is a complex solid-gas multiphase reaction process involving reactions in the solid, absorbed and gaseous phases. Several unsolved issues remain till now[40,41]. At low temperatures decomposition, the AP decomposes leading to formation of a small number of intermediate products, the main pivotal step is that the electrons transfer from perchlorate ion to ammonium ion, which would transfer to NH_3 and $HClO_4$ by dissociation and sublimation and as follows:
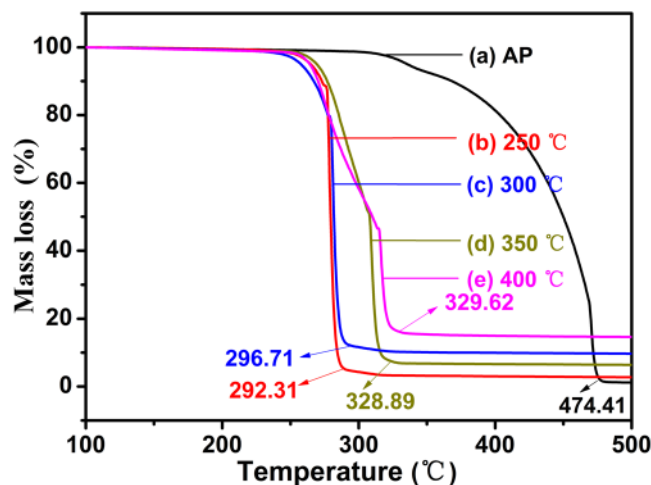
Figure 9. TG curves of the AP decomposition in the absence and presence of ZnCo$_2$O$_4$ rod at different calcined temperature at a 2% mass basis: (**a**) pure AP, (**b**) 250 ºC, (**c**) 300 ºC, (**d**) 350 ºC and (**e**) 400 ºC, respectively.
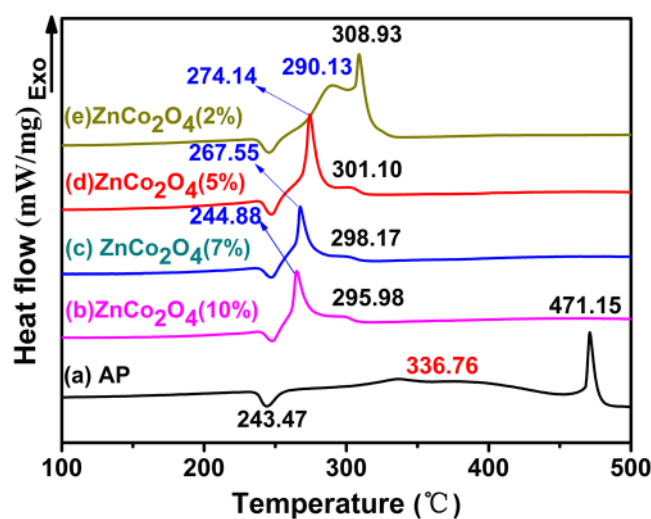

Figure 10. DSC curves of the AP decomposition in the presence of the ZnCo$_2$O$_4$ calcined at 250 ºC: (**a**) pure AP; (**b**) AP + ZnCo$_2$O$_4$(10%); (**c**) AP + ZnCo$_2$O$_4$(7%); (**d**) AP + ZnCo$_2$O$_4$(5%) (**e**) AP + ZnCo$_2$O$_4$(2%), respectively.

Materials	M%	β °C/min	LTD Peak (°C)		Decrease of LTD Peak (°C)	HTD Peak (°C)		Decrease of HTD Peak (°C)	Ref.
			Pure AP	AP+ Sample		Pure AP	AP+ Sample		
Nanoparticles MnFe$_2$O$_4$	3	20	328.7	289.2	39.54	430.2	345.3	84.9	5
Nanoparticles CuCr$_2$O$_4$	2	20	331			467	369.9	97.1	14
Nanorod ZnCo$_2$O$_4$	2	5	316.7	274.5	42.2	449.2	290.9	158.3	17
Nanopowders CuCo$_2$O$_4$	3	No description	331.1	308.43	22.71	443.6	340.8	102.8	13
Nanoparticles CoFe$_2$O$_4$	2	20	326.2	—	—	433.2	320.4	112.8	35
Nanoporous CoFe$_2$O$_4$	2	5	315.7	—	—	413.9	356.0	57.9	36
Microspheres Fe$_3$O$_4$	2	20	317	—	—	456	376	80	37
Microspheres Co$_3$O$_4$	2	20	317	—	—	456	382	74	
Nanometer CuFe$_2$O$_4$	2	10	333.3	318.4	14.9	445	353.8	91.2	38
Nanoparticles Co$_3$O$_4$	2	10	325	—	—	453.1	336.2	116.9	39
Porous ZnCo$_2$O$_4$ (250 °C)	2	20	336.7	290.13	46.55	471.2	309.1	162.01	This work

Table 3. Comparison of Catalytic activity for Ammonium Perchlorate of various transition metal oxides. **Notes:** In this table, M, β, LTD and HTD represent the blend ratio of catalysts, heating rate, low-temperature decomposition and high-temperature decomposition respectively.
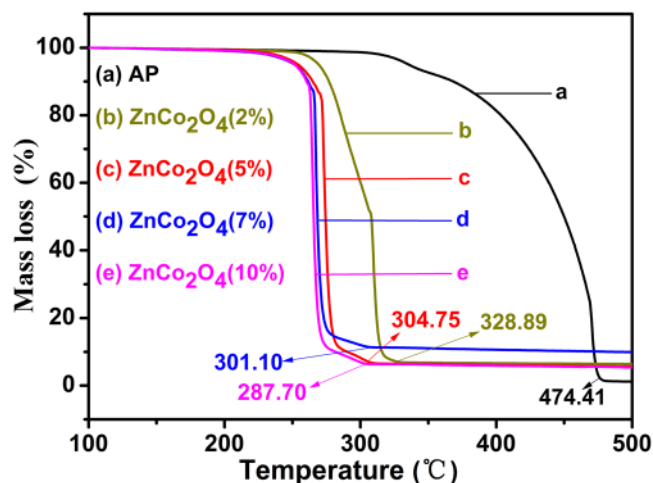
Figure 11. TG curves of the AP decomposition in the presence of the $ZnCo_2O_4$ calcined at 250 ℃: (**a**) pure AP; (**b**) AP + $ZnCo_2O_4$(2%); (**c**) AP + $ZnCo_2O_4$(5%); (**d**) AP + $ZnCo_2O_4$(7%) (**e**) AP + $ZnCo_2O_4$(10%), respectively.

$$NH_4ClO_4 \rightarrow ClO_4^- + NH_4^+ \rightarrow ClO_4^0 + NH_4^0 \rightarrow HClO_4 + NH_3 \tag{1}$$

Boldyrev *et al.* assumed the electrons transfer to happen on the surface not interior of crystal[42]. After the NH_4^+ accepts electron to become activated NH_4^0, the activated ammonium radicals can decompose to ammonia and hydrogen atom:

$$NH_4^0 \rightarrow NH_3 + H \tag{2}$$

The activated ClO_4^0 can react with hydrogen atom and form $HClO_4$, the $HClO_4$ can further reacted with the H atom:

$$HClO_4 + H \rightarrow ClO_3 + H_2O \tag{3}$$

As an electron absorption body, ClO_3 can converted into ClO_3^- which then react with NH_3 in the adsorbed gas to produce various such as NO, N_2O, H_2O[15]:

$$ClO_3 + e^- \rightarrow ClO_3^- \tag{4}$$

The intermediate products NH_3 and $HClO_4$ by dissociation and sublimation of AP are not only absorbed on the surface of perchlorate crystal to react, but also desorbed and sublimed into the gas phase[35]. Because the adsorbed NH_3 can not be completely oxidized by the decomposition products of $HClO_4$ at low temperature, it overlays continually on the surface of AP. Hence, the NH_3 adsorbed on the surface gets saturated, which causes cessation of the reaction and incomplete transformation of perchlorate. As the temperature rising sequentially, the reaction between NH_3 and $HClO_4$ absorbed on the surface of AP will be triggered again to produce final volatile products including HCl, H_2O, NO, N_2O and so on[43]. In the high-temperature decomposition process, the controlling step is the transformation from O_2 to superoxide ion O_2^-, which can further react with NH_3 to form N_2O, NO_2 and H_2O[44]. Therefore, the high electron transfer capacity and large specific surface area of the catalyst have an important effect on the thermal decomposition of AP. According to the electron transfer mechanism, the $ZnCo_2O_4$ as p-type semiconductor materials, it has effective sites (positive holes on the surface of catalyst) to accept released electron from perchlorate, accompanied by the abstraction of atomic oxygen from the perchlorate ion[45].

$$e^-_{oxide} + ClO_4^- \rightarrow O_{oxide} + ClO_3^- \rightarrow 1/2O_2 + e^-_{oxide} + ClO_3^- \tag{5}$$
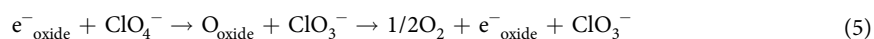
where e^-_{oxide} represents a positive hole in the valence band of the oxide and O_{oxide} is an abstracted oxygen atom from oxide. The mechanism of catalytic action is based on the presence of superoxide ion O_2^- on the surface of the catalysts, so the $ZnCo_2O_4$ catalyst may promoted the dissociation of ClO_4^- species into ClO_3^- and O_2. In addition, the transition metal ion Co^{3+} in the spinel structure of $ZnCo_2O_4$ has outermost d orbitals with $3d^6$ electronic configurations, and the d orbitals are not filled with electrons and have hole conductivity. It can easily accept the released electron from ClO_4^- to form Co^{2+} ($3d^7$) cations, the electron was transferred to the surface of the catalyst and reacted with NH_4^+ to decompose into ammonia and hydrogen atom[46].
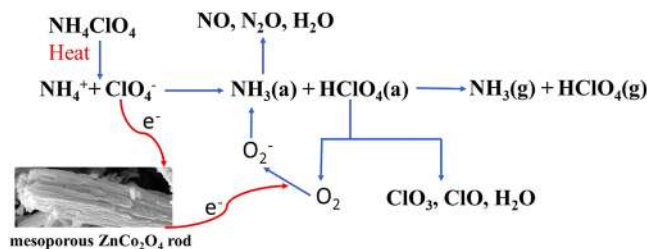
$$Co^{3+} + ClO_4^- \rightarrow Co^{2+} + ClO_4^0 \tag{6}$$

$$Co^{2+} + NH_4^+ \rightarrow Co^{3+} + NH_4^0 \tag{7}$$

Figure 12. Schematic diagram of the thermal catalytic activity enhancement of mesoporous $ZnCo_2O_4$ rod.
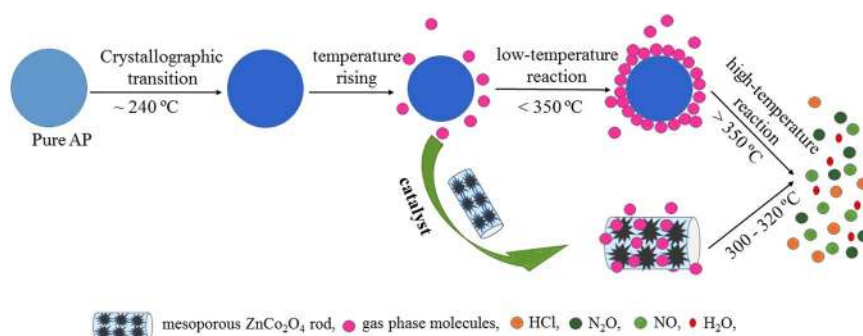

Figure 13. Flow diagram of the thermal decomposition process of AP in the absence and presence of mesoporous $ZnCo_2O_4$ rod.

In the thermal decomposition process of AP, $ZnCo_2O_4$ serves as a bridge for transferred electrons from perchlorate ions to the ammonium ions and the other transformation from O_2 to superoxide ion O_2^-, as depicted in Fig. 12. In the end, positive synergistic catalytic effect of ternary oxide may also contribute to AP's decomposition[13]. Due to the high specific surface area and great adsorption of the mesoporous $ZnCo_2O_4$ rods, the decomposed intermediate products in the gaseous phase of AP can be facilely adsorbed on the surface of mesoporous $ZnCo_2O_4$ rods shown in Fig. 13. Thus, the addition of mesoporous $ZnCo_2O_4$ to AP can increase the contact area of the catalytic reaction, augment the number of active sites, which promotes the thermal decomposition of AP. So that the mesoporous $ZnCo_2O_4$ rod calcined at 250 °C manifests highest catalytic activity than other products, which is mainly because of its relatively highest specific surface area.

Conclusions

In summary, mesoporous $ZnCo_2O_4$ rod has been successfully synthesized via a controlled thermal decomposition of homogeneous complex oxalates precursor, which is no need of the assistance of soft/hard template. XRD, SEM, TEM, XPS and nitrogen adsorption/desorption have been done to systematically characterize the structural and morphological features of the as-prepared products. After calcined at given temperature with a low rate of heating, the nano-sized $ZnCo_2O_4$ crystallites connected together to form mesoporous rod. The as-prepared material $ZnCo_2O_4$ calcined at 250 °C showed much larger surface area (102.34 $m^2 \cdot g^{-1}$) and high catalytic activity, shifting the AP high thermal decomposition temperature downwardly to about 162.1 °C. The results suggest that the as-prepared mesoporous $ZnCo_2O_4$ rod has great catalytic properties on thermal decomposition of AP, which can be used as a promising additive in the future.

References

1. Zhang, Y. F. *et al.* Fabrication of $V_3O_7 \cdot H_2O$@C core-shell nanostructured composites and the effect of $V_3O_7 \cdot H_2O$ and $V_3O_7 \cdot H_2O$@C on the decomposition of ammonium perchlorate. *J. Alloys Compd.* **509**, 69–73 (2011).
2. Zhang, Y. F. *et al.* Synthesis, characterization, and catalytic property of nanosized MgO flakes with different shapes. *J. Alloys Compd.* **590**, 373–379 (2014).
3. Hosseini, S. G. *et al.* Synthesis and characterization of α–Fe_2O_3 mesoporous using SBA-15 silica as template and investigation of its catalytic activity for thermal decomposition of ammonium perchlorate particles. *Powder Technol.* **278**, 316–322 (2015).
4. Mallick, L. *et al.* Thermal decomposition of ammonium perchlorate-A TGA-FTIR-MS study: Part I. *Thermochim. Acta* **610**, 57–68 (2015).
5. Han, A. J. *et al.* Preparation of nano-$MnFe_2O_4$ and its catatlytic performance of thermal decomposition of Ammonium perchlorate, Chin. *J. Chem. Eng.* **19**, 1047–1051 (2011).
6. Chen, L. J. *et al.* Synthesis of CuO nanorods and their catalytic activity in the thermal decomposition of ammonium and perchlorate. *J. Alloys Compd.* **464**, 532–536 (2008).
7. Chen, W. F. *et al.* Preparation of nanocrystalline Co_3O_4 and its catalytic performance for thermal decomposition of ammonium perchlorate. *Chinese Journal of catalysis* **26**, 1073–1077 (2005).
8. Wang, Y. P. *et al.* Preparation of NiO nanoparticles and their catalytic activity in the thermal decomposition of ammonium perchlorate. *Thermochim. Acta.* **437**, 106–109 (2005).
9. Tang, G. *et al.* The atomic origin of high catalytic activity of ZnO nanotetrapods for decomposition of ammonium perchlorate. *CrystEngComm.* **16**, 570–574 (2014).

10. Wojciechowska, M. *et al*. Copper-cobalt oxide catalysts supported on MgF$_2$ or Al$_2$O$_3$ —their structure and catalytic performance. *Applied Catalysis A: General* **298**, 225–231 (2006).
11. Cui, B. B. *et al*. Core-ring structured NiCo$_2$O$_4$ nanoplatelets: synthesis, characterization, and electrocatalytic appllications. *Adv. Funct. Mater.* **18**, 1440–1447 (2008).
12. Rosa-Toro, L. A. *et al*. Preparation and characterization of copper-doped cobalt oxide electrodes. *J. Phys. Chem. B.* **110**, 24021–24029 (2006).
13. Gheshlaghi, E. A. *et al*. Investigation of the catalytic activity of nano-sized CuO, Co$_3$O$_4$ and CuCo$_2$O$_4$ powders on thermal decomposition of ammonium perchlorate. *Powder Technol.* **217**, 330–339 (2012).
14. Patil, P. R. *et al*. Effect of nano-copper oxide and copper chromite on the thermal decomposition of ammonium perchlorate. *propellants, Explosives, Pyrotechnics* **33**, 266–270 (2008).
15. Eslami, A. *et al*. Fabrication of ammonium perchlorate/copper-chromium oxides core-shell nanocomposites for catalytic thermal decomposition of ammonium perchlorate. *Mater. Chem. Phys.* **181**, 12–20 (2016).
16. Deng, S. J. *et al*. Flash synthesis of macro-/nanoporous ZnCo$_2$O$_4$ via self-sustained decomposition of metal-organic complexes. *Mater. Lett.* **134**, 138–141 (2014).
17. Jia, Z. G. *et al*. A new precursor strategy to prepare ZnCo$_2$O$_4$ nanorods and their excellent catalytic activity for thermal decomposition of ammonium perchlorate. *Appl. Surf. Sci.* **270**, 312–318 (2013).
18. Deng, S. J. *et al*. Structure and catalytic activity of 3D macro/mesoporous Co$_3$O$_4$ for CO oxidation prepared by a facile self-sustained decomposition of metal-organic complexes. *J. Mol. Catal. A: Chem.* **398**, 79–85 (2015).
19. Li, G. N. *et al*. One-pot pyrolytic synthesis of mesoporous MCo$_2$O$_{4(4.5)}$ (M = Mn, Ni, Fe, Cu) spinels and its high efficient catalytic properties for CO oxidation at low temperature. *J. Mol. Catal. A: Chem.* **390**, 97–104 (2014).
20. Tomboc, G. M. *et al*. PVP assisted morphology-controlled synthesis of hierarchical mesoporous ZnCo$_2$O$_4$ nanoparticles for high-performance pseudocapacitor. *Chem. Eng. J.* **308**, 202–213 (2017).
21. Zhao, R. Z. *et al*. Highly ordered mesoporous spinel ZnCo$_2$O$_4$ as a high-performance anode material for lithium-ion batteries. *Electrochim. Acta* **197**, 58–67 (2016).
22. Feng, Y. J. *et al*. Controlled synthesis of highly active mesoporous Co$_3$O$_4$ polycrystals for low temperature CO oxidation. *Applied Catalysis B: Environmental.* **111–112**, 461–466 (2012).
23. Yu, C. C. *et al*. A simple template-free strategy to synthesize nanoporous manganese and nickel oxides with narrow pore size distribution, and their electrochemical properties. *Adv. Funct. Mater.* **18**, 1544–1554 (2008).
24. Pan, Y. *et al*. A facile synthesis of ZnCo$_2$O$_4$ nanocluster particles and the performance as anode materials for Lithium ion batteries. *Nano-Micro Letters.* **9**, 20 (2017).
25. Li, J. F. *et al*. Spinel Mn$_{1.5}$Co$_{1.5}$O$_4$ core-shell microspheres as Li-ion battery anode materials with a long cycle life and high capacity. *J. Mater. Chem.* **22**, 23254–23259 (2012).
26. Hao, S. J. *et al*. Synthesis of multimodal porous ZnCo$_2$O$_4$ and it electrochemical properties ad an anode material for lithium ion batteries,. *J. Power Sources.* **294**, 112–119 (2015).
27. Hu, L. L. *et al*. Facile synthesis of uniform mesoporous ZnCo$_2$O$_4$ microspheres as a high-performance anode material for Li-ion batteries. *J. Mater. Chem. A* **1**, 5596–5602 (2013).
28. Marco, J. F. *et al*. Characterization of the nickel cobaltite, NiCo$_2$O$_4$, prepared by several methods: an XRD, XANES, EXAFS, and XPS study. *J. Solid State Chem.* **153**, 74–81 (2000).
29. Prasad, R. *et al*. Low temperature complete combustion of a lean mixture of LPG emissions over cobaltite catalysts. *Catalysis Science & Technology* **3**, 3223–3233 (2013).
30. Kalman, J. *et al*. Nano-computed tomographic measurements of partially decomposed ammonium perchlorate particles. *Propellants, Explosives, Pyrotechnics.* **42**, 1111–1116 (2017).
31. Gross, M. L. *et al*. Coupling micro and meso-scale combustion models of AP/HTPB propellants. *Combust. Flame.* **160**, 982–992 (2013).
32. Venkatachalam, V. *et al*. Double hydroxide mediated synthesis of nanostructured ZnCo$_2$O$_4$ as high performance electrode material for supercapacitor applications. *Chem. Eng. J.* **321**, 474–483 (2017).
33. Compos, E. A. *et al*. Chemical and textural characterization of iron oxide nanoparticles and their effect on the thermal decomposition of ammonium perchlorate. *Propellants, Explosives, Pyrotechnics.* **40**, 860–866 (2015).
34. Said, A. A. *et al*. The role of copper cobaltite spine, Cu$_X$Co$_{3-X}$O$_4$ during the thermal decomposition of ammonium perchlorate. *Thermochim. Acta.* **275**, 83–91 (1996).
35. Zhao, S. S. *et al*. Preparation of CoFe$_2$O$_4$ nanocrystallites by solvothermal process and its catalytic activity on the thermal decomposition of ammonium perchlorate. *J. Nanomater.* **842816**, 1–5 (2010).
36. Xiong, W. H. *et al*. Preparation of nanoporous CoFe$_2$O$_4$ and its catalytic performance during the thermal decomposition of ammonium perchlorate. *Acta Physico-Chimica Sinica.* **32**, 2093–2100 (2016).
37. Zhang, Y. F. *et al*. Facile fabrication of Fe$_3$O$_4$ and Co$_3$O$_4$ microspheres and their influence on the thermal decomposition of ammonium perchlorate. *J. Alloys Compd.* **674**, 259–265 (2016).
38. Liu, T. *et al*. Preparation of nanometer CuFe$_2$O$_4$ by auto-combustion and its catalytic activity on the thermal decomposition of ammonium perchlorate. *Mater. Lett.* **62**, 4056–4058 (2008).
39. Hosseini, S. G. *et al*. The effect of average particle size of nano-Co$_3$O$_4$ on the catalytic thermal decomposition of ammonium perchlorate particles. *J. Therm. Ana. Calorim.* **124**, 1243–1254 (2016).
40. Wang, J. *et al*. Controlled synthesis of Co$_3$O$_4$ single-crystalline nanofilms enclosed by (111) facets and their exceptional activity for the catalytic decomposition of ammonium perchlorate. *CrystEngComm.* **16**, 8673–8677 (2014).
41. Cheng, Z. P. *et al*. Synthesis of flower-like and dendritic platinum nanostructures with excellent catalytic activities on thermal decomposition of ammonium perchlorate. *Mater. Res. Bull.* **77**, 54–59 (2016).
42. Boldyrev, V. V. *et al*. Thermal decomposition of ammonium perchlorate. *Thermochim. Acta.* **443**, 1–36 (2006).
43. Liu, D. *et al*. Polyoxometalate-based purely inorganic porous frameworks with selective adsorption and oxidative catalysis functionalities. *Chem. Commun.* **49**, 3673–3675 (2013).
44. Wang, J. X. *et al*. Enhanced thermal decomposition properties of ammonium perchlorate through addition of 3DOM core-shell Fe$_2$O$_3$/Co$_3$O$_4$ composite. *J. Alloys Compd.* **724**, 720–727 (2017).
45. Kumar, H. *et al*. The effect of reduced graphene oxide on the catalytic activity of Cu-Cr-O-TiO$_2$ to enhance the thermal decomposition rate of ammonium perchlorate: an efficient fuel oxidizer for solid rocket motors and missiles. *ARC. Advances.* **7**, 36594–36604 (2017).
46. Wang, Y. P. *et al*. Catalytic activity of nanometer-sized CuO/Fe$_2$O$_3$ on thermal decomposition of AP and combustion of AP- based propellant. *Combust. Sci. Technol.* **183**, 154–162 (2010).

Acknowledgements

Author Contributions

The research was planned by Y.D.W. Experiments were performed by X.C.X., B.G.P., L.F.C. X.M.Z. and S.R.L. X.C.X. and Y.D.W. prepared the manuscript. B.G.P., L.F.C., X.M.Z. and S.R.L. involved in the scientific discussions. All the authors participated in discussing and reviewing of the manuscript.

Additional Information

Supplementary information accompanies this paper at https://doi.org/10.1038/s41598-018-26022-2.

Competing Interests: The authors declare no competing interests.

Publisher's note: Springer Nature remains neutral with regard to jurisdictional claims in published maps and institutional affiliations.